Pergamon

J. Aerosol Sci., Vol. 26, No. 6, pp. 933–944, 1995

0021-8502/95 $9.50 + 0.00

0021-8502(95)00028-3

ASPIRATION EFFICIENCY OF A THIN-WALLED SHALLOW-TAPERED SAMPLER REAR-FACING THE WIND

D. B. Ingham,* X. Wen,* N. Dombrowski† and E. A. Foumeny†

* Department of Applied Mathematical Studies, † Department of Chemical Engineering, University of Leeds, Leeds LS2 9JT, U.K.

(*First received* 14 *December* 1994; *and in final form* 13 *March* 1995)

Abstract—The aspiration efficiency of a thin-walled, shallow-tapered aerosol sampler, as studied by Vincent *et al.* (1986, *J. Aerosol Sci.* **17**, 211–224), which is rear-facing the wind is numerically investigated. The turbulent fluid flow is predicted by employing the control volume, finite-difference method with a body-fitted coordinate system and a low Reynolds number k–ε turbulence model. The particle trajectories are calculated by integrating the particle equations of motion using either the turbulent instantaneous fluid velocity (a stochastic model) or the mean fluid motion (the mean motion model). The aspiration efficiency for thin-walled, shallow-tapered samplers which rear-face the wind as predicted by the two models, are in good agreement and although the results show an unusual behaviour they agree reasonably well with all the available experimental data.

INTRODUCTION

Thin-walled sampling probes are used primarily for duct sampling in order to determine the concentration of particles in relevant size fractions in the ambient atmosphere and in clean rooms. The early experimental work and theoretical analysis concentrated on the situation when the sampler faces the wind, and the probe diameter is less than 25 mm, see for example Badzioch (1959), Vitols (1966), Sehmel (1967), Ruping (1968), Belyaev and Levin (1974), Jayasekera and Davies (1980) and Okazaki *et al.* (1987).

When the orientation angle of the sampler to the wind is in the region from 0° to 90° experimental work and semi-theoretical-empirical analyses have been performed by Durham and Lundgren (1980), Davies and Subari (1982), Vincent *et al.* (1986), Hangal and Willeke (1990) and Grinshpun *et al.* (1993). For an orientation angle of 180°, only Vincent *et al.* (1986) have experimentally investigated thin-walled samplers but more recently Tsai and Vincent (1993) have theoretically extended the impaction model of Vincent (1987, 1989) to thin-walled, blunt samplers which are rear-facing the wind. Dunnett (1990) performed a numerical investigation on thin-walled samplers at orientations with respect to the flow direction from 0° to 90° by employing a potential fluid flow model and more recently Wen and Ingham (1994) have presented a numerical investigation on the sampling mechanism for thin-walled cylindrical samplers using the turbulent k–ε model (see Launder and Spalding, 1974).

In this paper the numerical investigation of Wen and Ingham (1994) has been extended to thin-walled, shallow-tapered samplers which are rear-facing the wind. A low Reynolds number turbulent k–ε model has been used in order to simulate the turbulent air flow in the sublayer of the boundary-layer on the wall of the sampler. The particle paths have been traced by considering the averaged turbulent fluid velocity (the mean motion model) or the turbulent instantaneous fluid velocity (the stochastic model) in which the fluctuating turbulent fluid velocity is locally isotropic with a Gaussian distribution.

MATHEMATICAL MODEL

The sampler under investigation is cylindrical, thin-walled and shallow-tapered and has the same dimensions as the sampler employed in the experimental work of Vincent *et al.* (1986), see Fig. 1 for a schematic diagram of the sampler investigated. The sampler consists of a long shallow-tapered probe of circular cross-sectional area. The probe is of diameter

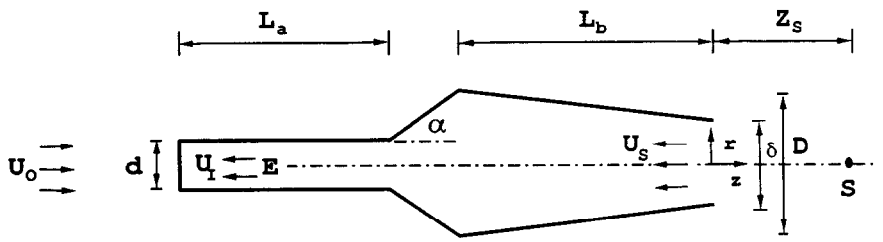

Fig. 1. A schematic diagram of a thin-walled, shallow-tapered sampler which is rear-facing the oncoming wind. (a) $\delta = 2.0$ cm, $D = 7.0$ cm, $U_s = 2.0\,\mathrm{m\,s^{-1}}$, $U_0 = 2.0\,\mathrm{m\,s^{-1}}$. (b) $\delta = 5.0$ cm, $D = 7.0$ cm, $U_s = 2.0\,\mathrm{m\,s^{-1}}$, $U_0 = 2.0\,\mathrm{m\,s^{-1}}$.

δ at the orifice, diameter D at its base and of length L_b. The probe is connected to a cylindrical pipe of diameter d at its base by means of a shoulder which is inclined to the axis of the sampler at an angle α. Cylindrical coordinates are used in which r is the coordinate in the radial direction and z is aligned with the axis of symmetry of the sampler and is measured positively from the plane of the orifice of the sampler in the direction of the undisturbed freestream flow U_0. At the orifice of the sampler the fluid enters the sampler with an average sampling velocity U_s. A large distance along the cylindrical pipe the fluid flow becomes fully developed turbulent flow, with an average sampling velocity U_i, and we assume that this takes place at the section E, see Fig. 1. Therefore we define the ratio of the undisturbed fluid velocity to the average sampling velocity at the orifice as the velocity ratio $R = U_0/U_s$ and the ratio of the diameter of the probe at the orifice to its diameter at its base as the sampler ratio $r_1 = \delta/D$. Because some of the oncoming fluid enters the sampler and some will not, there is a dividing stream surface which separates these fluids. In particular there is a point on the axis of symmetry of the sampler where there is a stagnation point, say the point S, see Fig. 1, and the distance from stagnation point S to the orifice of the sampling probe is assumed to be Z_s.

In this paper, to match the experimental operating conditions in the wind tunnel of Vincent *et al.* (1986) we have assumed that the air flow is turbulent. Clearly, the geometry of the sampler is more complex than the cylindrical sampler which was considered by Wen and Ingham (1994), with the consequence that the air flow around the sampler is also more distorted. Given the geometry of the sampler, the flow is characterized by the Reynolds number $\mathrm{Re} = U_0\delta/\nu$, where ν is the kinematic viscosity of the air. In most experimental situations, and in particular those investigated by Vincent *et al.* (1986), the Reynolds numbers are typically of the order 4000 and the thickness of the turbulent boundary-layer is of the same order as that of the diameter of the orifice of the sampler. In this situation the standard k–ε model cannot reveal the true nature of the fluid flow by using the wall function in regions very close to the wall of the sampler. Therefore, in this paper we use a 'low Reynolds number turbulent k–ε model', for further details see, for example, Launder and Sharma (1974).

For an incompressible fluid, the momentum and the continuity equations for turbulent fluid flow, in vector notation, are given by

$$\mathbf{V}\cdot\nabla\mathbf{V} = -\frac{1}{\rho}\nabla p + \nabla\cdot(\nu_e\nabla\mathbf{V}), \tag{1}$$

$$\nabla\cdot\mathbf{V} = 0, \tag{2}$$

where $\mathbf{V} = u\mathbf{e}_r + w\mathbf{e}_z$, u and w are the mean values of the turbulent components of the fluid velocity in the radial and axial directions, respectively, and $\mathbf{e}_r$ and $\mathbf{e}_z$ are the unit vectors in the radial and axial directions, respectively, ρ is the density of the fluid and ν_e is the effective kinematic viscosity of the fluid and consists of the sum of the laminar kinematic viscosity ν and the turbulent kinematic viscosity ν_t, i.e. $\nu_e = \nu + \nu_t$.

A low Reynolds number turbulent k–ε model, developed by Launder and Sharma (1974), is given by

$$(\mathbf{V}\cdot\nabla)k = \nabla\cdot\left[\left(\nu + \frac{\nu_t}{\sigma_k}\right)\nabla k\right] + \phi - \varepsilon + E_1, \tag{3}$$

$$(\mathbf{V}\cdot\nabla)\varepsilon = \nabla\cdot\left[\left(\nu + \frac{\nu_t}{\sigma_\varepsilon}\right)\nabla\varepsilon\right] + C_1 f_1 \frac{\varepsilon}{k}\phi - C_2 f_2 \frac{\varepsilon^2}{k} + E, \tag{4}$$

where k is the turbulent kinetic energy, ε is the turbulent energy dissipation, ϕ is the generation of the turbulent energy which is caused by turbulent stresses, and

$$f_1 = 1.0, \tag{5}$$

$$f_2 = 1 - 0.3\exp(-R_T^2), \tag{6}$$

$$R_T^2 = k^2/\nu\varepsilon, \tag{7}$$

$$E = 2\nu\left(\frac{\partial k^{1/2}}{\partial x_j}\right)^2, \tag{8}$$

$$E_1 = -2.0\nu\nu_t\left(\frac{\partial^2 U_i}{\partial x_j \partial x_1}\right). \tag{9}$$

The turbulent viscosity ν_t is given by

$$\nu_t = C_\mu f_\mu \frac{k^2}{\varepsilon}, \tag{10}$$

where

$$f_\mu = \exp\left(\frac{-3.4}{(1 + R_T/50)^2}\right). \tag{11}$$

Further, the coefficients which occur in equations (3)–(11) should be determined by performing an experimental investigation on the flow around the sampler. However, there is a severe lack of detailed measurements on the turbulent velocity distribution, and of other turbulence quantities, for flows around samplers. Therefore, the values of the unknown coefficients used in this paper are those suggested by Launder and Sharma (1974), namely,

$$C_\mu = 0.09, \quad \sigma_k = 1.0, \quad \sigma_\varepsilon = 1.3, \quad C_1 = 1.44, \quad C_2 = 1.92. \tag{12}$$

These values are based on a very extensive examination of various fluid flows and form the best available data.

In order to solve for the fluid velocity, the turbulent kinetic energy k and the turbulent dissipation ε, the control volume, finite-difference method is used in order to discretize equations (1)–(4), see Ingham and Wen (1993), using body-fitted coordinates and a non-staggered grid. Different body-fitted coordinates, mesh sizes and solution domains have been investigated in order to obtain accurate numerical results and we found that an orthogonal coordinate system with 170×80 grid nodes which covers the region of $-11.7(D/2) \leqslant z \leqslant 8.4(D/2)$, $0 \leqslant r \leqslant 10(D/2)$ can produce reliable numerical results. The resulting algebraic equations were solved using a line-by-line Tridiagonal-Matrix Algorithm. The SIMPLEC algorithm (see Van Doormaal and Raithby, 1984), which is a modification to the SIMPLE algorithm (see Patankar, 1980), and the average velocity and pressure correction technique (see Wen and Ingham, 1993) is employed. The upstream values for the turbulent kinetic energy and dissipation were specified, namely $k = (IU_0)^2$ and $\varepsilon = C_\mu^{3/4}k^{1.5}/L$, where I is the turbulent intensity and L is the turbulent length scale. In the experimental investigation of Vincent *et al.* (1986) they estimated that the value of I was 0.06 and $L = 7$ cm. Therefore all the calculations presented in this paper were performed with these values of I and L.

Stochastic model

When the particle density is much larger than that of air and the particle Reynolds number is much less than unity, then the i component of the Lagrangian particle equation of motion takes the form

$$\frac{\mathrm{d}x_i}{\mathrm{d}t} = u_{pi}, \tag{13}$$

$$\frac{\gamma^* d_{ae}^2}{18\mu}\frac{\mathrm{d}u_{pi}}{\mathrm{d}t} = \bar{u}_i + u_i' - u_{pi}, \tag{14}$$

where γ^* is the density of water, d_{ae} is the particle aerodynamic diameter, μ is the viscosity of the fluid, x_i normalised by $\delta/2$ is the position of the particle, u_{pi} is the i component of the velocity of the particle, $\bar{u}_i$ is the mean fluid velocity of the fluid and u_i' is the fluctuating component of the fluid velocity, u_{pi}, $\bar{u}_i$ and u_i' are normalised by U_0. The Stokes number is defined as

$$\mathrm{St} = \gamma^* d_{ae}^2 U_0/(18\mu\delta/2). \tag{15}$$

The motion of the particles are not equally affected by the different scales of turbulence, but rather the motion is mainly governed by the interaction of the particle with a succession of large eddies, each of which is assumed to have constant flow properties. A method for tracking the particle motion was developed by Gosman and Ioannides (1981) assuming that the velocity fluctuations are isotropic and have a Gaussian distribution with a standard deviation given by

$$u_e = (2k/3)^{1/2}. \tag{16}$$

Thus the fluctuating velocity components are given by

$$u_i' = \Psi_i u_e/U_0, \tag{17}$$

where Ψ_i are normally distributed pseudorandom numbers and u_i' is used in the particle equation (14) to evaluate the instantaneous drag force on the particle. The length scale L_e and the lifetime τ_e of the large scale eddies are, see for example Gosman and Ioannides (1981) and Shuen *et al.* (1983), given by

$$L_e = C_\mu^{3/4} k^{1.5}/\varepsilon, \qquad \tau_e = L_e/u_e, \tag{18}$$

respectively.

The transit time required for the particle to cross the eddy was determined by Shuen *et al.* (1983) for a particle in a uniform flow, i.e.

$$\tau_t = -\tau \ln\{1 - L_e/[\tau|(u_1^2 + u_2^2)^{1/2} - (u_{p1}^2 + u_{p2}^2)^{1/2}|]\}, \tag{19}$$

where τ is the relaxation time of the particle, namely

$$\tau = d_{ae}^2 \gamma^*/18\mu. \tag{20}$$

Equations (13) and (14), which govern the motion of the particles, were integrated over the time T, which is the minimum of the eddy lifetime and the transit time, i.e. $T = \min\{\tau_e, \tau_t\}$.

The calculation of the aspiration efficiency has been performed in two simple situations, namely, for both sticky and non-sticky walls. When the wall of the sampler is considered not to be sticky, it is assumed that when particles impact on the wall of the sampler they bounce off and the coefficient of restitution is defined as $\beta = V_2/V_1$, where V_2 is the normal component of the rebound velocity and V_1 is normal component of the impact velocity. When the wall of the sampler is considered to be sticky, it is assumed that once a particle impacts on the wall of the sampler it sticks to the wall. In practice once a particle hits the surface of the sampler it is possible that it will be reentrained into the flow by means of blow-off and this is influenced more by the nature of the air flow and drag forces on the particle in the boundary-layer and less by the speed of the impact of the particle. Because

this phenomena is complex and the inclusion of blow-off depends on numerous other independent quantities it is not included in the present work. However, the situations of a sticky wall and perfect impaction gives the two extremes for the aspiration efficiency. The aspiration efficiency will lie between these limits. But in most practical situations, the 'sticky-wall' assumption is the closest to reality.

In order to obtain the dispersion properties of the particles a number M ($M = 1000$ has been taken in all the results presented in this paper in order to obtain a stable statistic value of P) of particles of a given size were released at the same point at a large distance upstream of the sampler. Then the probability that the particle is sampled for this size of particles is defined as

$$P = \frac{N}{M}, \tag{21}$$

where N is the number of sampled particles. Clearly, P is a function of Q_r, where Q_r is the flux of fluid across the area enclosed by the circle in the plane of constant z on which the particles start. It has been assumed that far upstream of the sampler the particle has the same velocity as that of the air and the concentration of particles of a given size is constant. Thus the aspiration efficiency of the sampler is given by the expression

$$A = \frac{\int_0^\infty P(Q_r)\,\mathrm{d}Q_r}{Q}, \tag{22}$$

where Q is the sampled flux of air which enters the sampling probe.

Mean motion model

In general the turbulent fluctuating air velocity is much smaller than the average air velocity and under the assumption of local isotopic turbulence, a particle has an equal chance of diffusing in the two directions which are normal to the mean particle motion. Therefore, when there exists a uniform concentration of particles at large distances from the sampler it is expected that the inertia of the particle will be more important than the particle diffusion in the determination of the aspiration efficiency. Therefore if we neglect the effect of particle diffusion on the aspiration efficiency of the sampler, i.e. we neglect the fluctuations in the fluid velocity, then equation (14) simplifies to

$$\frac{\gamma^* d_{ae}^2}{18\mu}\frac{\mathrm{d}u_{pi}}{\mathrm{d}t} = \bar{u}_i - u_{pi}. \tag{23}$$

Further, based on equation (23), for a given particle size there exists a particle limiting surface. The particles within the limiting particle surface will be sampled and the particles outside of the limiting particle surface will not be sampled. Thus the aspiration efficiency of the sampler is given by the expression

$$A = Q_0/Q, \tag{24}$$

where Q_0 is the flux of air which is enclosed by the particle limiting surface far upstream of the sampler and Q is the sampled flux of air which enters the sampling probe.

The stochastic model and the mean motion model were used to evaluate the aspiration efficiency for the two thin-walled, shallow-tapered samplers which were experimentally investigated by Vincent *et al.* (1986). These samplers have the same size of sampler body, $L_b = 13.0$ cm and $D = 7.0$ cm, the same size of arm, $L_a = 8.5$ cm, $d = 1.0$ cm and $\alpha = 45°$, but have different orifice diameters, namely $\delta = 2.0$ and 5.0 cm. Calculations have been performed with the oncoming wind speeds of $U_0 = 1.0$, 2.0 and 3.8 m s^{-1} and this gives rise to sampling velocity ratios $R = U_0/U_s = 0.67$, 1.0 and 2.0, respectively. The value of these parameters were chosen so as to correspond to the experimental conditions of Vincent *et al.* (1986).

RESULTS AND DISCUSSIONS

In order to reveal the general characteristics of the turbulent air flow in the vicinity of the sampler, the velocity vectors and the streamlines are shown in Fig. 2 for the two samplers with diameters $\delta = 2$ cm and $\delta = 5$ cm under the operating condition of $U_0 = 2.0\ \mathrm{m\,s^{-1}}$ and $R = 1.0$. It is observed that the air flows are significantly distorted near the arm of the sampler. Further, as the flow approaches the body of the sampler the air is displaced by the body of the sampler. It is in the vicinity of the bluntest section of the sampler that the air

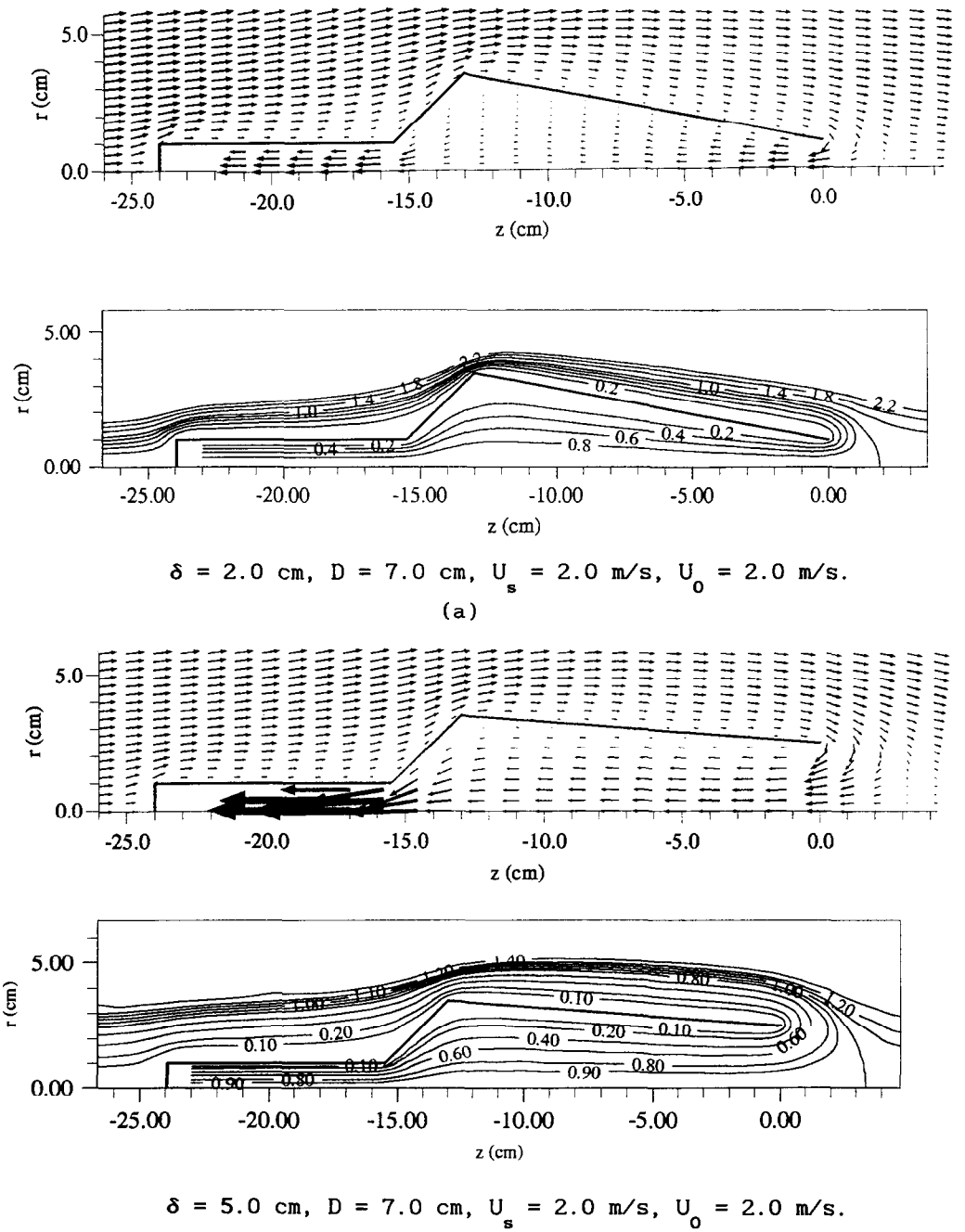

Fig. 2. Velocity vectors and streamlines in the vicinity of the sampler when $R = 1.0$, $U_0 = 2.0\ \mathrm{m\,s^{-1}}$ for (a) $\delta = 2.0$ cm and (b) $\delta = 5.0$ cm.

velocity is largest and where the boundary-layer on the external wall of the sampler has a minimum thickness. Beyond the bluntest section of the sampler the air begins to converge towards the orifice of the sampler and the smaller sampler orifice causes a sharper distortion of the streamlines near to the orifice than does the larger sampler orifice. When the air is in the region which is less than a distance of about one radius of the orifice of the sampler from the orifice of the sampler it undergoes a rapid acceleration, due to the action of the sampling, and in this vicinity the boundary-layer thickness is sharply reduced in size. Downstream of the orifice of the sampler the air which is contained in the limiting stream surface is sucked back into the sampler, and in the vicinity of the orifice of the sampler the air undergoes a rapid change in its direction of flow. The air then continues to flow into the sampling probe and eventually becomes the fully developed turbulent flow in the circular exit pipe. The sampler also draws air from the boundary-layer along the external wall of the sampler and this illustrates that the sampling process is very complex when the sampler is rear-facing the wind.

Both the stochastic model and the mean motion model have been employed to calculate the aspiration efficiency of the sampler. Figure 3 shows the variation of the probability that a particle is sampled as a function of Q_r/Q when $\delta = 2.0$ cm, $U_0 = 2.0\ \mathrm{m\,s^{-1}}$, $R = 1.0$, and $\mathrm{St} = 0.002$. It is observed that when $Q_r/Q \leqslant 0.93$ then $P(Q_r/Q)$ takes a value of 1.0, and this means that all the particles which start within a circle which has a radius of $\sqrt{0.93}\delta$ and centre on the z axis are sampled. Otherwise when $Q_r/Q \geqslant 0.93$ the value of $P(Q_r/Q)$ begins to decrease and is close to the value of zero when $Q_r/Q = 1.1$, namely when all particles which start outside a circle which has its centre on the z-axis and has a radius of $\sqrt{1.1}\delta$ are not sampled. In this case the radius of the limiting surface upstream is $\sqrt{0.978}\delta$ and this implies that some of the particles which are within the particle limiting surface are not sampled but some particles which are outside of the particle limiting surface are still sampled because of particle diffusion. Because the value of Q_r is proportional to r^2, the particles which are outside of the particle limiting surface respond to a larger flux of fluid and therefore the aspiration efficiency produced by the stochastic model will always be slightly larger than that produced by the mean motion model. We have also performed numerous calculations for $0.002 \leqslant \mathrm{St} \leqslant 1.0$ and found that the aspiration efficiency produced by the stochastic model is consistently slightly larger than that produced by the mean motion model by an amount up to about 0.05 for all the values of the Stokes number, St, considered. It is also worth noticing that when the Stokes number is very small the stochastic model produces an aspiration efficiency which is larger than unity. Therefore, we conclude that the stochastic model used in this paper gives results for the aspiration efficiency which are not significantly different from those predicted by the mean motion model. However, in order to produce the aspiration efficiency under the same operating conditions the stochastic model takes approximately 100 times longer to obtain results than does the mean motion model.

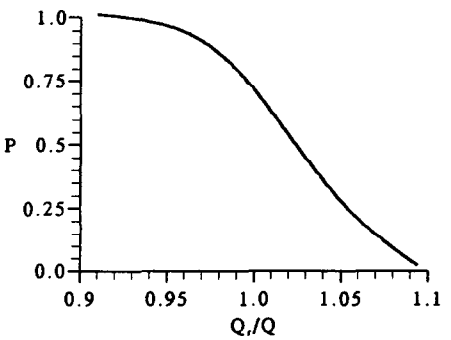

Fig. 3. The variation of the probability that particles are sampled as a function of Q_r/Q for $U_0 = 2.0\ \mathrm{m\,s^{-1}}$, $R = 1.0$, $D = 7.0$ cm, $\delta = 2.0$ cm and $\mathrm{St} = 0.002$.

Therefore in the remainder of this paper we present results for the aspiration efficiency using only the mean motion model.

When considering the interaction between the particles and the wall of the sampler as a perfect elastic impaction, namely, $\beta = 1.0$, Fig. 4 shows that the aspiration efficiency A as a function of the Stokes number, St, when $U_0 = 1.0$, 2.0 and 3.8 m s^{-1}, i.e. $R = 0.67$, 1.0 and 2.0, for the two samplers investigated experimentally by Vincent *et al.* (1986) and comparisons have also been made with the experimental data. We observed that when the Stokes number is very small the limiting particle surface is very close to the limiting streamline surface. Increasing the Stokes number causes the limiting particle surface to move closer to

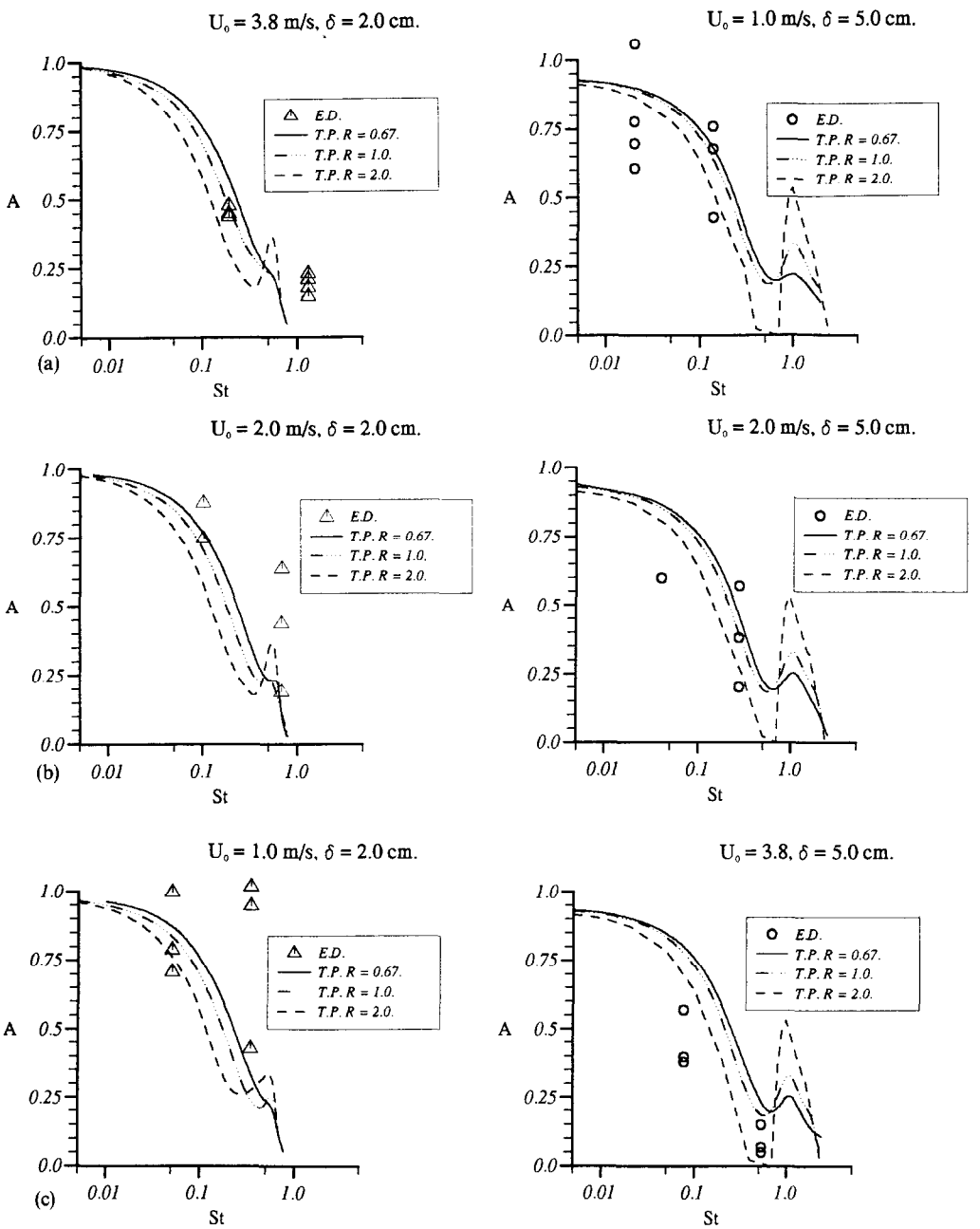

Fig. 4. The variation of the aspiration efficiency as a function of the Stokes number. (a) $U_0 = 3.8$ m s^{-1}, (b) $U_0 = 2.0$ m s^{-1}, and (c) $U_0 = 1.0$ m s^{-1}. The experimental data have been taken from Table 3 of Vincent *et al.* (1986). (E.D.—Experimental Data; T.P.—Theoretical Prediction.)

the body of the sampler. Therefore all the numerical and experimental data show that the aspiration efficiency steadily decreases as the Stokes number increases. Among the sampled particles, some have impacted on the external wall of the sampler but some will pass around the bluntest section of the sampler without bouncing on the wall. It is very interesting to observe that the aspiration efficiency has a minimum value. The reason for this is that for Stokes numbers less than where the minimum aspiration occurs the limiting particle surface insects the upstream face of the sampler. In this situation all the particles within the limiting particle surface impact on the wall of the sampler and rebound back into the air flow field. This leads to a reduction in the axial component of the particle velocity and consequently the inertia of the particle in the axial direction is reduced. However, as the Stokes number increases further the aspiration efficiency sharply decreases and the particles of large size will not be sampled, although the axial component of the particle velocity has been reduced by the impact on the wall. We also observe that when the ratio δ/D is small (say when $\delta = 2.0$ cm) the impaction of the particle on the wall of the sampler has less effect on the aspiration efficiency than it does for larger values of δ/D (say when $\delta = 5.0$ cm). This is because after the particles pass around the bluntest section of the sampler they are further from the external wall of the sampler, due to their inertia, and therefore the boundary-layer along the external wall of the sampler has less effect on the motion of the particle. When the value of δ/D is larger then, after the particles have passed around the bluntest section of the sampler, the particles are closer to the external wall of the sampler and the boundary-layer along the external wall of the sampler slows down the motion of the particle. This leads to a larger aspiration efficiency. Further, when the Stokes number is large the experimental data also show an increase in the aspiration efficiency and this is consistent with our numerical predictions.

The numerical predictions of the aspiration show that as the value of R decreases, the aspiration efficiency increases. In Fig. 4 we have not marked the experimental data according to the value of R because for fixed values of δ/D and U_0 there are only four or five experimental data points available and this is not sufficient to reveal the variation of the aspiration efficiency with the value of R. We also observe that the freestream velocity has little effect on the aspiration efficiency. However, the smaller the orifice of the sampler then the smaller is the aspiration efficiency. A possible reason for this could be that the geometries from the arm to the bluntest section of the sampler are the same for the two samplers in our calculations but may not be in the experimental investigation. Thus, the velocity distributions around the arm and the bluntest section are similar and this results in the efficiencies being almost the same. However, the smaller the value of δ/D the smaller is the aspiration efficiency.

When the impaction of the particles on the external wall of the sampler is not perfect, numerical calculations have also been performed for the coefficient of restitution $\beta = 0.5$. Figure 5a shows the aspiration efficiency as a function of the Stokes number for the smaller sampler orifice diameter, namely $\delta = 2.0$ cm, and hence $\delta/D = 2/7$. The results for the perfect impaction are also presented in this figure under the same sampling operation conditions. The numerical results show that the aspiration efficiency rapidly increases when all of the sampled particles have impacted on the wall and the smaller the coefficient of restitution, the larger is the aspiration efficiency. This rapid increase in the aspiration efficiency only occurs in a small range of values of the Stokes number and on further increasing the Stokes number then no particles are sampled. Figure 5b shows the aspiration efficiency as a function of the Stokes number for the larger sampler orifice diameter, namely $\delta = 5.0$ cm and hence $\delta/D = 5/7$. We observe that for this larger value of δ/D then the coefficient of restitution, β, has a much more significant effect on the aspiration efficiency than it does at the smaller value of δ/D. This comparison leads us to conclude that as the value of δ/D decreases, the effect of the coefficient of restitution on the aspiration efficiency decreases.

When the external wall of the sampler is perfectly sticky, i.e when a particle hits the wall it sticks to it, the numerical calculations have been performed for $D = 7.0$ cm, $\delta = 5.0$ cm, $U_0 = 2.0\ \mathrm{m\,s^{-1}}$ and Fig. 6 shows that the aspiration efficiencies as a function of the Stokes

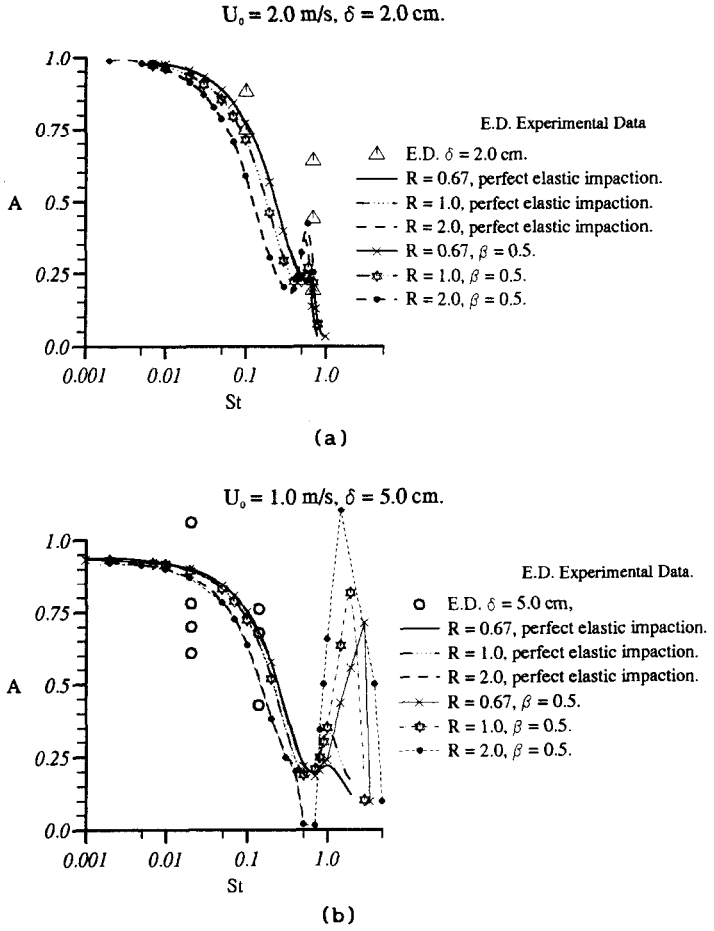

Fig. 5. The effect of the coefficient of restitution on the aspiration efficiency when $\delta = 2.0$ cm and (a) $\delta/D = 2/7$, (b) $\delta/D = 5/7$.

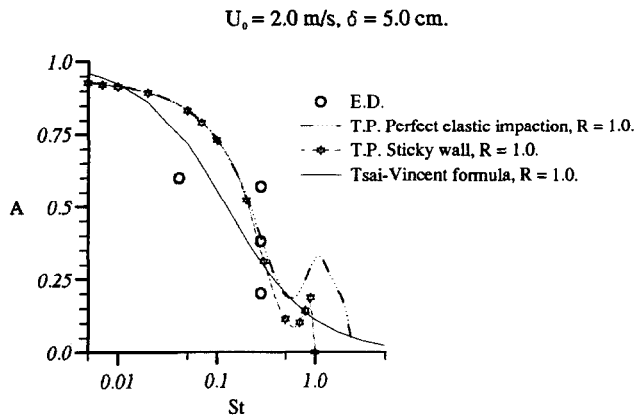

Fig. 6. A comparison of the results obtained using the impaction model, perfectly elastic impaction, perfectly sticky wall and the experimental data when $U_0 = 2.0\ \mathrm{m\,s^{-1}}$, $\delta = 5.0$ cm, $D = 5.0$ cm and $R = 1.0$ for the aspiration efficiency.

number when $R = 1.0$. A comparison is also made for a sticky wall, perfect impaction and the Tsai–Vincent formula. It is observed that the aspiration efficiencies predicted by the numerical model are in reasonable agreement with the predictions of Vincent's impaction model. It is also observed that when the Stokes number is large, the perfectly sticky wall

predicts a smaller aspiration efficiency than the Tsai–Vincent formula and this is because in practice not all the particles which hit the wall will stick to it. Further, the perfect elastic impaction produces a larger aspiration efficiency than the impaction model of Vincent and this is because in the numerical model the transverse shift produced by such as particle rotation, large averaged turbulent velocity gradients near the wall and the non-isotropism of the fluctuations in the fluid velocities are ignored. Therefore, in practice the aspiration efficiency will lie between those predicted by the perfectly sticky wall and the perfectly elastic impaction models.

CONCLUSIONS

Thin-walled, shallow-tapered samplers, as investigated by Vincent *et al.* (1986), have been investigated for a large range of conditions which occur in actual air environments, when the samplers are placed at an angle of inclination of 180° to the oncoming air flow using a low Reynolds turbulent k–ε model. It has been found that the stochastic model for particle diffusion gives results for the aspiration efficiency of the sampler which are not substantially different from those predicted using the mean motion model. However, it is interesting to note that the stochastic model, which is very expensive in CPU time, predicts an aspiration efficiency which is slightly greater than unity when the Stokes number is very small. In general, both the models numerically predict aspiration efficiencies which agree reasonably well with all the available experimental data and the Tsai–Vincent formula.

We conclude, for thin-walled, shallow-tapered samplers as investigated in this paper that:

(a) The inertia of the particles, namely, the particle Stokes number, St, dominates the sampling process.

(b) The sampling velocity ratio and the impaction of the particles on the wall of the sampler have a significant effect on the aspiration efficiency when the Stokes number is close to unity.

(c) A decrease in the ratio of the diameter, δ, of the orifice of the sampler to the diameter, D, of the sampler, i.e. δ/D, produces a decrease in the aspiration efficiency.

(d) The turbulent boundary-layer flow along the external wall of the sampler has a significant effect on the sampling efficiency when the Stokes number is close to unity and the value of δ/D is large.

(e) The larger the velocity ratio, U_0/U_s, the smaller is the aspiration efficiency.

(f) Much experimental data for the aspiration efficiency of samplers which rear-face the wind is required and further numerical investigations should be performed according to the dimensions of the sampler employed in these experiments.

Acknowledgement—The authors gratefully acknowledge the financial support of the Health and Safety Executive and EPSRC.

REFERENCES

Badzioch, S. (1959) Collection of gas-borne dust particles by means of an aspirated sampling nozzle. *Br. J. appl. Phys.* **10**, 26–32.

Belyaev, S. P. and Levin, L. M. (1974) Techniques for collection of representative aerosol samplers. *J. Aerosol Sci.* **5**, 325–338.

Davies, C. N. and Subari, M. (1982) Aspiration above wind velocity of aerosols with thin-walled nozzles facing and at right angles to the wind direction. *J. Aerosol Sci.* **13**, 59–71.

Dunnett, S. J. (1990) Mathematical modelling of aerosol sampling with thin-walled probes at yaw orientation with respect to the wind. *J. Aerosol Sci.* **21**, 947–956.

Durham, M. D. and Lundgren, D. A. (1980) Evaluation of aerosol aspiration efficiency as a function of Stokes' number, velocity ratio and nozzle angle. *J. Aerosol Sci.* **11**, 179–188.

Gosman, A. D. and Ioannides, E. (1981) Aspects of computer simulation of liquid-fueled combustors. *AIAA Paper* No. 81-0323.

Grinshpun, S., Willeke, K. and Kalatoor, S. (1993) A general equation for aerosol aspiration by thin-walled sampling probes in calm and moving air. *Atmos. Envir.* **27A**, 1459–1470, with the Corrigendum, **28A**, 375 (1994).

Hangal, S. and Willeke, K. (1990) Aspiration efficiency: unified model for all forward sampling angles. *Environ. Sci. Technol.* **24**, 688–691.

Ingham, D. B. and Wen, X. (1993) Disklike body sampling in a turbulent wind. *J. Aerosol Sci.* **24,** 629–642.
Jayasekera, P. N. and Davies, C. N. (1980) Aspiration below wind velocity of aerosols with sharp-edged nozzles facing the wind. *J. Aerosol Sci.* **11,** 535–547.
Launder, B. E. and Sharma, B. I. (1974) Application of the energy-dissipation model of turbulence to the calculation of flow near a spinning disc. *Lett. Heat Mass Transfer* **1,** 131–138.
Launder, B. E. and Spalding, D. B. (1974) The numerical computation of turbulent flows. *Comput. Methods appl. mech. Engng* **3,** 269–289.
Okazaki K., Wiener, R. W. and Eilleeke, K. (1987) Nonisoaxial aerosol sampling mechanisms controlling the overall sampling efficiency. *Environ. Sci. Technol.* **21,** 183–187.
Patankar, S. V. (1980) *Numerical Heat Transfer and Fluid Flow.* Hemisphere, Washington, DC.
Ruping, G. (1968) *Staub-Reinlalt. Luft* **28,** 1 (English translation).
Sehmel, G. A. (1967) Velocity of air samplers as affected by anisokinetic sampling and deposition within sampling line, *Proc. of the Symposium on Assessment of Airborne Radioactivity,* Vienna, pp. 727–735.
Shuen, J.-S., Chen, L.-D. and Faeth, G. M. (1983) Evaluation of a stochastic model of particle dispersion in a turbulent round jet. *A.I.Ch.E. J.* **29,** 167–170.
Tsai, P.-J. and Vincent. J. H. (1993) Impaction model for the aspiration efficiencies of aerosol samplers at large angles with respect to the wind. *J. Aerosol Sci.* **24,** 919–928.
Van Doormaal, J. P. and Raithby, G. D. (1984) Enhancements of the SIMPLE method for predicting incompressible fluid flows. *Numer. Heat Transfer* **7,** 147–163.
Vincent, J. H. (1987) Recent advances in aspiration theory for thin-walled and blunt aerosol sampling probes. *J. Aerosol Sci.* **18,** 487–498.
Vincent, J. H. (1989) *Aerosol Sampling: Science and Practice.* Wiley, Chichester.
Vincent, J. H., Stevens, D. C., Mark, D., Marshall M. and Smith T. A. (1986) On the aspiration characteristics of large-diameter, thin-walled aerosol sampling probes at yaw orientations with respect to the wind. *J. Aerosol Sci.* **17,** 211–224.
Vitols, V. (1966) Theoretical limits of errors due to anisokinetic sampling of particulate matter. *J. Air Pollut. Control Assoc.* **16,** 79–84.
Wen, X. and Ingham, D. B. (1993) A new method for accelerating the rate of convergence of the SIMPLE-like algorithm. *Int. J. numer. Methods Fluids* **7,** 385–400.
Wen, X. and Ingham, D. B. (1994) Aerosol sampling from a thin-walled cylindrical probe at a yaw orientation of 180°. *J. Aerosol Sci.* **26,** 95–107.